coatings

MDPI

Article

Hypothesis on the Influence of the Magnetic Behaviour of Hydrogen Doped Zinc Oxide during its Plasma Sputtering Process

A. Salimian *, A. Hasnath, A. Aminishahsavarani and H. Upadhyaya *

Centre for Advanced Materials, School of Engineering, London South Bank University, 103 Borough Road, London SE1 0AA, UK; hasnatha@lsbu.ac.uk (A.H.); aminisha@lsbu.ac.uk (A.A.)
* Correspondence: salimiaa@lsbu.ac.uk (A.S.); upadhyah@lsbu.ac.uk (H.U.)

Abstract: We investigate the complexity of the reactive sputtering of highly conductive zinc oxide thin films in the presence of hydrogen at room temperature. We report on the importance of precise geometric positioning of the substrate with respect to the magnetron to achieve maximum conductivity. We examine the electrical properties of the deposited thins films based on their position on the substrate holder relative to the magnetron. By considering early reports by other researchers on the angular dependency of plasma parameters and the effect of hydrogen doping on electric and magnetic properties of hydrogen-doped zinc oxide, we propose a hypothesis on the possibility of such properties resulting in the observations presented in this report pending further tests to verify this hypothesis. Overall, in this report we present the guide by which highly conductive zinc oxide thin film coatings can be prepared via RF sputtering with hydrogen presence along with argon as the sputtering gas.

Keywords: sputtering, zinc oxide, magnetic, TCO, hydrogen doping

Citation: Salimian, A.; Hasnath, A.; Aminishahsavarani, A.; Upadhyaya, H. Hypothesis on the Influence of the Magnetic Behaviour of Hydrogen Doped Zinc Oxide during Its Plasma Sputtering Process. *Coatings* **2021**, *11*, 222. https://doi.org/10.3390/coatings11020222

Academic Editor: Alessandro Patelli
Received: 30 December 2020
Accepted: 9 February 2021
Published: 13 February 2021

1. Introduction

Transparent conductive oxides (TCOs) are materials that show both transparency and conductivity, with applications in solar cells, optoelectronics, electroluminescent panels and various flat panel displays, as reported in various studies [1–7]. A band gap of above 3.3 eV and electrical conductivity in the range of 10^4 S·cm^{-1} (Siemens per centimetre) are the fundamental aspects of such materials. Various oxides behave as TCOs among which indium tin oxide (ITO) is the dominant commercial type [8]. Another TCO material of choice is indium zinc oxide (IZO), with applications such as transparent electrodes in heterojunction thin film solar cell structures [9–13].

Indium is the fundamental material incorporated in many of these TCOs (apart from fluorine doped tin oxide), and the high price of indium and its short global supply impacts the economics of products associated with this family of TCOs. Hence, an alternative chemical composition that eliminates indium from these materials while maintaining their conductivity and transparency will bear significant commercial potential. Many binary and ternary oxide systems formed from the p-block metals demonstrate transparent conductive properties, such as CdO, Ga_2O_2, PbO_2, $CdSnO_3$, Sb_2O_2, ZnO, etc. [14,15].

Zinc oxide can be a potential alternative as it has the cheapest and most abundant atomic constituents with no significant toxicity associated with elements such as cadmium or lead. However, pure zinc oxide does not possess the required electrical properties to match those of IZO or ITO. Doping zinc oxide with hydrogen is a cheaper option that can significantly improve the conductivity of this material, and this was initially observed in 1950s [16,17].

The mechanism by which hydrogen incorporation into the zinc oxide lattice promotes n-type conductivity was theoretically investigated by van de Walle by first principal calculations based on density functional theory [18]. The behaviour of interstitial hydrogen in zinc oxide was studied by van de Walle, and the formation energy of H^+, H^-, H^0 and H_2 states in bonding centre and anti-bonding locations were evaluated, where H^+ demonstrated the lowest formation energy. The study showed that with incorporation of the hydrogen, an O–H bond forms along the direction of the original O–Zn bond. The strength of the O–H bond is the main driving force for stabilisation of the low energy H^+ configuration. Van De Walle concluded that H^+ is the stable charge state for all Fermi level positions in ZnO and acts as a donor [18]. The formation energy of the H+ was shown to be low enough to allow for large solubility of hydrogen in ZnO. It is interesting to note that hydrogen is amphoteric in other semiconductors, although not in ZnO. This difference is due to the strong O–H bond, which lowers the formation energy of H+. Parallel to this, a complex consisting of an oxygen vacancy and a hydrogen atom acts as a shallow donor. Such vacancies are low energy defects [19] and neutral, but the hydrogen turns them into a shallow donor, and as such, a hydrogen located close to the centre of such oxygen vacancies acts as a substitutional impurity [18]. These theoretical observations were then verified by electron nuclear double resonance and Muon spin spectroscopy [20,21]. The Fermi energy level where the positive and negative charge states are equal in energy occurs above the conduction band minimum in ZnO [22]. Thus, overall we can see that in a ZnO system, hydrogen acts as donor atom as H^+, providing the lattice with an extra electron as a charge carrier, which in turn makes ZnO an n-type material and influences the conductivity of the material.

However, apart from carrier density, the mobility of the charge carriers is an even more important feature of a potential conductor. Mobility is the measure of the velocity of carriers under an electric field and is inversely proportional to the effective mass of the charge carrier. The effective mass is inversely proportional to the second derivative of energy with respect to the k-vector in an E–k plot indicating how the electron states are spaced in k-space. E-k plot is the curvature of the energy band in a way that the larger curvature of the energy band translates to a smaller effective mass of the charge carrier [23]. The energy value computed in the E–k plot is governed by the orbital overlap of adjacent atoms, where the larger the orbital overlap is, the larger will be the drift of the charge carrier.

Parallel to the electrical properties of hydrogen-doped zinc oxide, several reported studies indicate doping of ZnO with hydrogen gives ferromagnetic properties to ZnO [24–26].

Hydrogenated ZnO nanoparticles are reported to demonstrate ferromagnetism because due to low formation energies, the formation of Zn vacancies and OH bonding by hydrogen is favoured in the hydrogenation process, leading to a magnetic moment of ~0.57 μB (Bohr magneton), and the origin of ferromagnetism is explained through the hydrogenation of the ZnO polar surface [27,28].

There are some experimental reports on electrical conductivity improvements achieved in the ZnO system with the addition of hydrogen with respect to TCO materials. However, such reports only exist at the research state, and no commercial TCO based on pure ZnO doped with hydrogen is present in the market to the best of our knowledge. We recently reported on enhancing the electrical properties of IZO and ZnO systems by repeated exposure of the sputtering target to an argon/hydrogen mixture as the working gas [29]. We have now identified interesting complexities associated with reactive hydrogen/argon sputtering of un-doped ZnO targets, which we believe are associated with the reported magnetic properties of hydrogenated ZnO particles, and this report outlines our observations.

The authors recently reported on implementing a novel approach through which the sputtering plasma can be given a unique fingerprint based on the colour of the plasma, which is identical to the method by which colour functions of a light source are expressed in a "x" and "y" coordinate system to define the unique colour of the light source [30]. We applied this technique for monitoring the plasma during these experiments and attempted to explain our observation by evaluating the colour parameters of the plasma in association with the electrical properties of the ZnO thin films deposited via reactive hydrogen/argon sputtering.

2. Experimental

The sputtering instrument used for these experiments was a V6000 unit that was manufactured by Scientific Vacuum Systems limited (SVS Ltd., Wokingham, UK) with a vacuum chamber with dimensions of ~40 cm × 40 cm × 40 cm with three 6" confocal targets. The distance between the target surface and substrate (centre to centre) was 15 cm at a 45° angle. The working gas used in the experiment was an argon–5% hydrogen (Ar + H) single source; the flow rate of the Ar + H gas for achieving the desired working pressure in the samples was adjusted accordingly, and sets of chamber pressures were used to deposit films associated with 13.9, 10 and 6 sccm Ar + H flow rates resulting in working chamber pressures of 0.3, 0.23 and 0.15 Pa. The depositions were carried out under 100, 150 and 200 watts of RF (radio frequency) plasma power under each flow rate.

The magnetron of the V6000 unit was fitted with a six-inch diameter of 99.99% pure zinc oxide (ZnO) target material with a copper indium back bond for efficient thermal dissipation, and all the depositions were performed at ambient temperature for a period of three hours. The focus of this report is the presentation of our observation on depositing highly conductive zinc oxide films via RF sputtering. We try to explain our observations by proposing a hypothesis based on earlier reports by other researchers on electrical and magnetic properties of zinc oxide materials doped with hydrogen. However, it needs to be clear that our hypothetical explanation will require further detailed examinations beyond the scope of the current article, as will be discussed.

2.1. Thin Film Deposition

The substrates were 1 mm thick soda lime glass slides 10 mm × 10 mm in dimension. All soda lime glass substrates were washed and sonicated with hellmanex, deionized water, acetone and ethanol separately inside a laminar flow station equipped with HEPA filters and then left to dry under vacuum to ensure a clean surface prior to thin film deposition. The substrates were placed on the substrate holder of the machine, as depicted in Figure 1, with position E indicating a substrate on the edge of the substrate holder, and C indicating the centre of the substrate holder position. The substrate was rotating at a speed of 10 rpm in all experiments. Using this configuration of substrate positions, thin films of ZnO were deposited under various amounts of plasma power and Ar + H flow rates in square cubic centimetre per minute (sccm). Table 1 presents the regime by which samples were prepared and named, where each deposition was carried out for a period of 3 h. In practice, we also placed glass samples in between the C and E positions; however, here we primarily focus on detailed observations associated with the E and C positions.

Table 1. Nine depositions were carried out under various plasma power and gas flow rates: high(H) flow rate (13.9 sccm), medium(M) flow rate (10 sccm) and low (L) flow rate (6 sccm), with substrates positioned at centre and edge of the substrate holder generating 18 total samples. E: refers to samples on the edge and C: refers to samples positioned on the centre of the substrate holder.

Sample Name	Position on substrate holder	Plasma Power (w)	Gas flow rate(sccm)
E100H	E	100	13.9(H)
E100M	E	100	10(M)
E100L	E	100	6(L)
E150H	E	150	13.9(H)
E150M	E	150	10(M)
E150L	E	150	6(L)
E200H	E	200	13.9(H)
E200M	E	200	10(M)
E200L	E	200	6(L)
C100H	C	100	13.9(H)
C100M	C	100	10(M)
C100L	C	100	6(L)
C150H	C	150	13.9(H)
C150M	C	150	10(M)
C150L	C	150	6(L)
C200H	C	200	13.9(H)
C200M	C	200	10(M)
C200L	C	200	6(L)

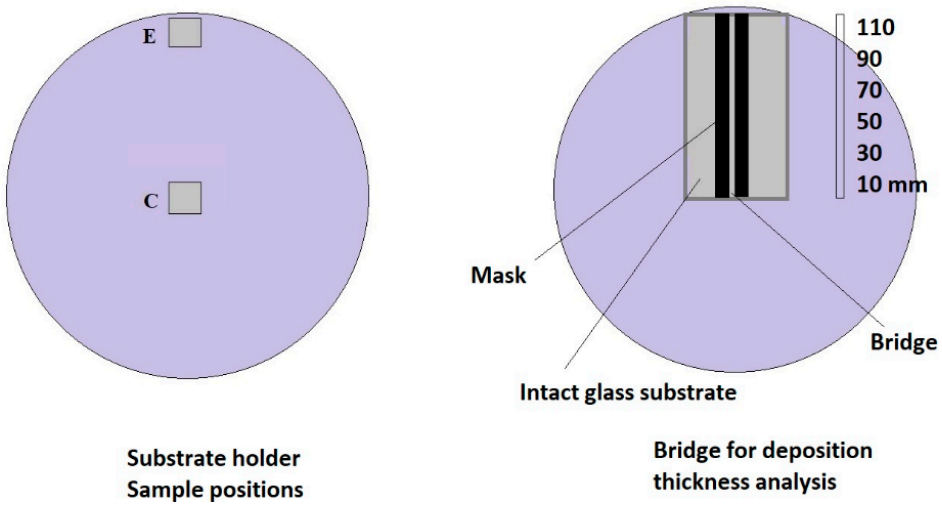

Figure 1. During each of the nine deposition trials, two soda lime glass samples were placed on the substrate holder (220 mm diameter), one in the centre and one on the edge (**left**). To measure the thickness gradient from the centre to the edge, a bridge between two masks was designated on an intact glass substrate for profilometric measurements; thickness of the samples was measured at the (10–110 mm) distance from centre, as depicted in this figure (**right**).

2.2. Spectral Data Collection from the Plasma Emissions

To obtain the spectral emission data and the colour function parameters of the plasma, an in-vacuum collimator optic probe that was made by Plasus GmbH (Mering, Germany) was placed on the substrate holder, as depicted in Figure 2, in such a way that data was collected from the centre and the edge of the target material fitted on the magnetron. Emission data collection was carried out under the exact same plasma conditions as the deposited samples were prepared. The data were collected in short periods to minimize the error that may result from the coating of the collimator quartz window (few seconds). At the same time, the quartz window was also fitted with a honey-comb gate guard that minimizes the coating of the quartz window. After each process, the collimator was dismantled and cleaned. UV–Vis spectroscopy was used, as described previously [30], to ensure that the coating of the quartz window would not cause significant error on the data collection process.

Emicon software (Version:4.11.1.2 ,Plasus GmbH, Mering, Germany) coupled to the spectrometer was programmed to calculate the area under the emission peaks (integral) of the spectral range based on pre-designated (300 nm to 900 nm in steps of 100 nm) segments of the spectrum. Parallel to the Plasus spectrometer, a Jeti Specbos 1201 spectrometer (Jena, Germany) was utilized to collect the spectral data to calculate the chromaticity index of the plasma light; the Jeti spectrometer was programmed so that for each measurement, it took 20 readings and inputted the average value of the x and y colour coordinates of the plasma light.

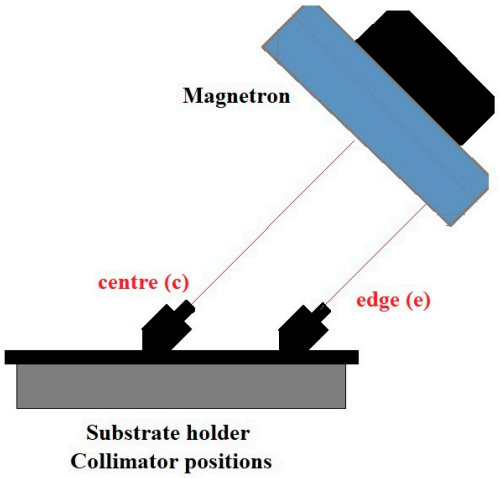

Figure 2. The collimator of the spectrometer was positioned on the substrate holder (centre and edge) to monitor the emissions of the sputtering plasma from the surface of the target fitted on the magnetron. The emission photons captured by the collimator were guided via a fibre optic cable to the spectrometer.

2.3. Sample Characterization

The samples were then tested for film thickness via a profilometer (Veeco, NY, USA), which was carried out by scanning the stylus of the profilometer over the one millimetre bridge gap coated on the intact glass sample, as depicted in Figure 1. The thickness was measure at 10, 30, 50, 70, 90 and 110 mm away from the centre of the substrate holder. Optical properties of the thin films were carried out via a UV–Vis spectrometer (Bibby Scientific Ltd., Staffs, UK) by using the absorption data. Tauc plots were made to measure the optical bandgap of the materials. The plot was made by plotting the hv(x-axis) against the $(ahv)^{1/r}$ (y-axis), where a is the absorption coefficient of the material. We chose the r-value = 2 for indirect allowed transitions.

Charge carrier density and mobility were measured by a home-built Hall effect measurements system, with 10 mm × 10 mm substrate sizes and the electrode pads connected to the four corners of the surface (~1 mm into the sample from the corner edge).

3. Results and Discussion

3.1. Electrical Properties

The ZnO coated substrates were tested for their electrical properties via a four-point probe and Hall effect measurement equipment. In this report, no study was carried out on the crystal structure of the deposited thin films; however, in a previous report where we examined similar samples of zinc oxide thin films deposited in the presence of hydrogen, the ZnO films were fully crystalline, showing the hexagonal ZnO zincite phase (PDF 01-075-1533) with a (101) preferential orientation [29].

The results indicated that the presence of hydrogen in the sputtering gas induces n-type conductivity by enhancing the concentration and mobility of the charge carriers (electrons). However, we can see that there is significant variation when comparing results between the samples positioned at the edge and centre of the substrate holder, as indicated in Figure 3.

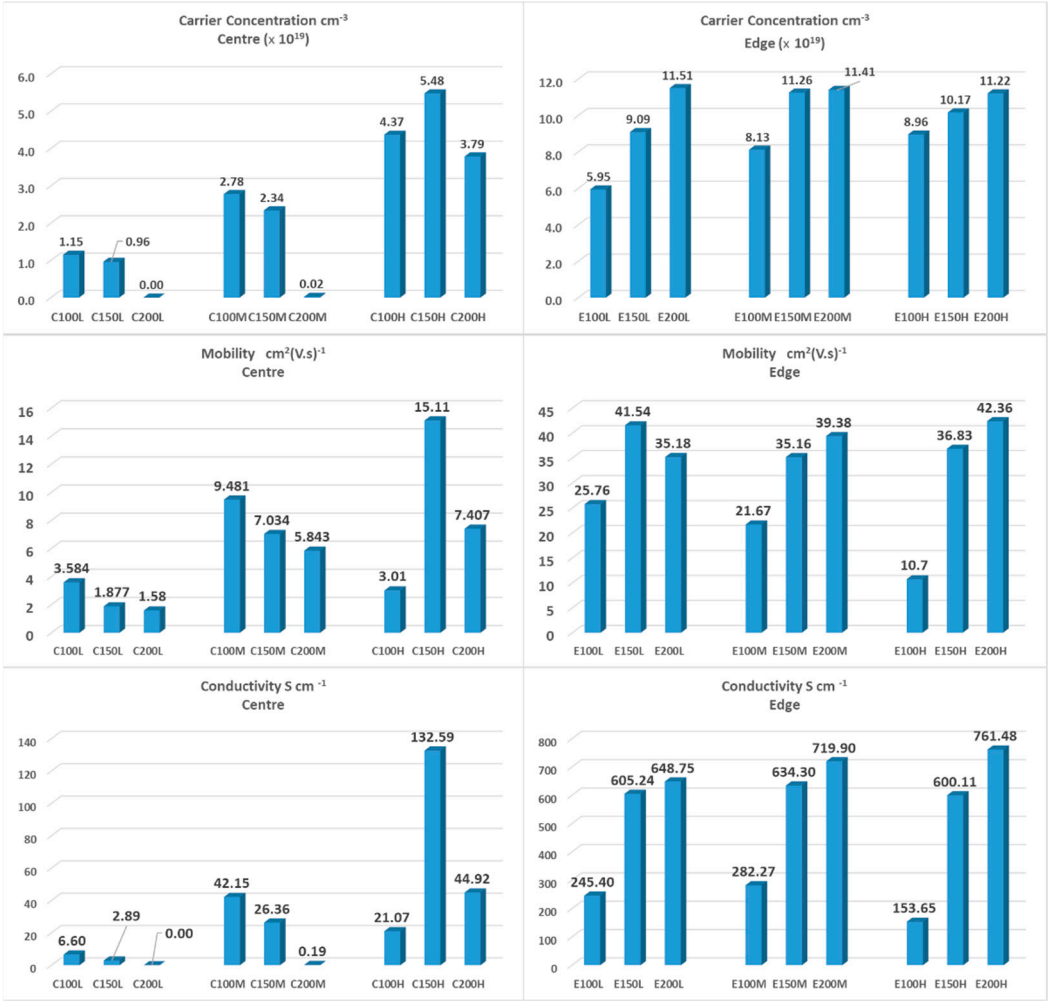

Figure 3. Carrier concentration and mobility were measured for ZnO samples deposited in the centre (**left**) and the edge (**right**) of the substrate holder under various plasma power and chamber pressures. The electrical properties of the deposited samples on the edge of the substrate are significantly superior to those of the depositions at the centre.

Charge carrier mobility and the carrier concentration are important in determining the electrical conductivity of a material, and we can see that high carrier concentration and mobility values are associated with the samples at the edge of substrate holder, while depositions at the centre demonstrate smaller values, and as such the overall conductivity of the edge samples are much higher. The mobility of the carriers is a function of carrier recombination time within the material while the carrier concentration is related to the carrier density. The carrier density in turn is the product of density of states and probability of occupancy. As previously discussed, the hydrogen impurity behaves as a donor in these samples. Associating higher conductivity to hydrogen integration into the lattice based on the discussed literature, the results can possibly indicate lower hydrogen content in the films prepared at the centre of the substrate holder, although this hydrogen content needs to be measured in future work to be perfectly conclusive. As discussed, we also placed substrates between the edge and centre regions. These samples were tested via a four-point probe measurement (Jandel, Leighton, UK) only, and we observed a conductivity gradient such that as we moved from the edge to the centre of the sample holder, the electrical property of the thin films became smaller. Based on our ongoing studies comparing IZO and ZnO, this is only observed in ZnO samples. To demonstrate a comparison for this report, we repeated the experiment with an IZO target fitted on the magnetron, and only the sheet resistance of the films was measured for presentation in this report. These results, presented in Figure 4, indicated that IZO does not behave like ZnO.

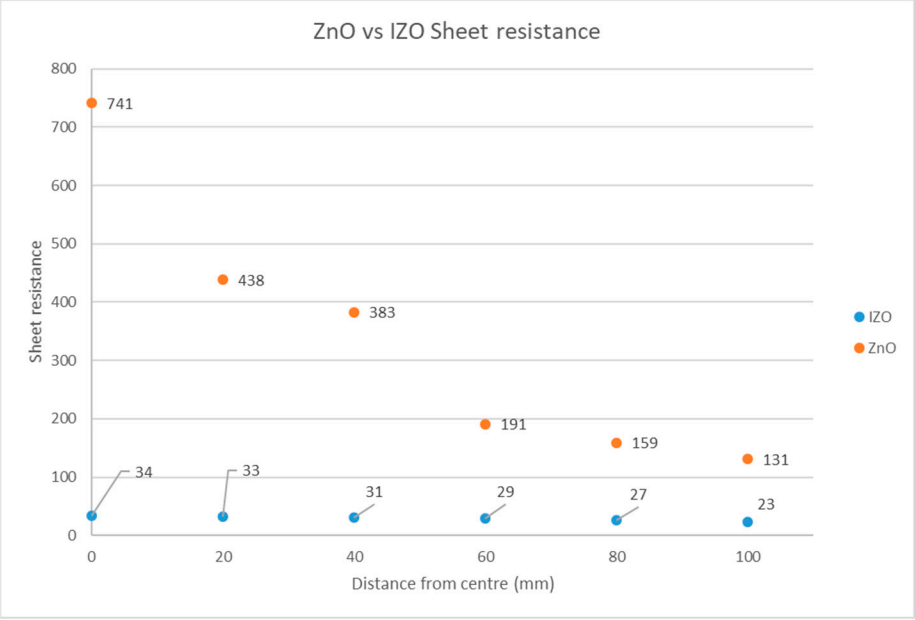

Figure 4. The sheet resistance (Ω□) of thin films of ZnO and IZO coated under exact conditions (100 W plasma power, 10 sccm Ar + H flow rate). The distance from the centre indicates the position of the glass substrate, and the readings are associated with the sheet resistance of the films.

As can be seen from the results presented in Figure 4, the electrical properties of the deposited films significantly varied for ZnO, depending on the position for the substrate, while for IZO the variation was significantly less elaborated (comparing the associated edge and centre samples). In a previous study, we demonstrated the enhanced electrical properties of the IZO when deposited under the argon–hydrogen mix [29]. These results combined with the observations presented in Figure 3 suggest that one way to explain this is to assume that more hydrogen doping is occurring at the edge of the substrate compared to the centre, unless the thickness of the coating was causing this observation. However, in the next section we show that thickness is not a relevant explanation for this observation.

The mobility of electrons through a solid is affected by local forces within the crystal structure. This mobility is then interpreted as the mass of the electrons within that crystal environment. In a ZnO crystal structure, the orbital overlap between the Zn cation and the oxygen anions can be an important factor in determining the above-mentioned electron mass due to the s-character of the cation at the conduction band [31]. We can hypothesize that when hydrogen is present as a sputtering gas, it may interact with the oxygen content of the lattice and result in localised lower oxygen contents, which will consecutively lead to predominant s-characteristics. This hypothesis is based on previously reported studies demonstrating the hydrogen to be a strong reducing gas in a plasma [32], while withdrawing oxygen from the In_2O_3 crystals during the deposition process has been reported to play a role of a doubly charged donor [33,34]. However, this cannot clearly explain the variation observed in edge and centre samples. Sheet resistance of edge and centre prepared ZnO samples are presented in Figure 5.

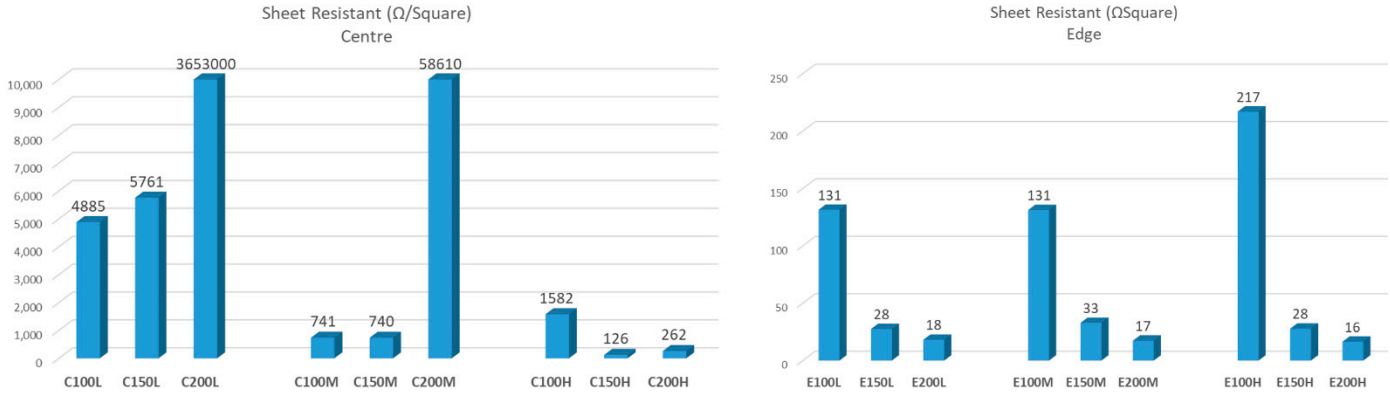

Figure 5. The sheet resistance (Ω square) of the ZnO samples deposited on the edge (**right**) and centre (**left**) part of the substrate holder under various deposition conditions.

3.2. Film Thickness and Optical Properties

The thickness of the coatings obtained via the profilometer in line with the sample preparation described in Figure 1 are presented in Figure 6 for all the ZnO samples.

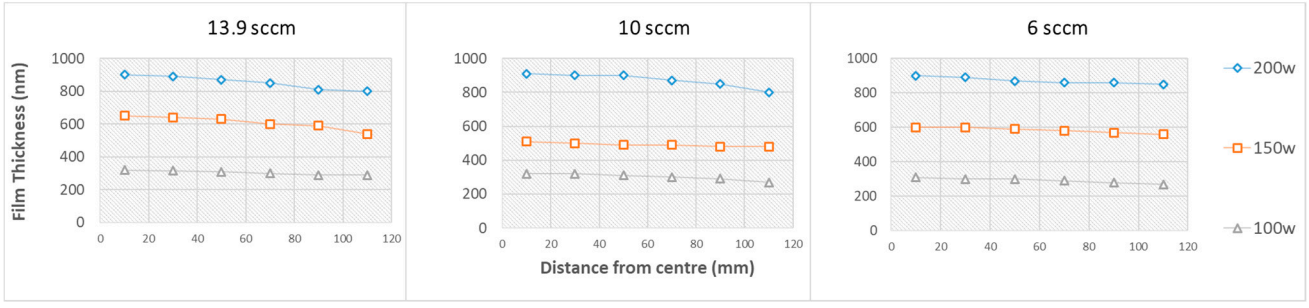

Figure 6. The coating thickness associated with the position of the substrate on the substrate holder (at a distance from the centre) under the varying deposition parameters; power and gas flow rate.

From Figure 6 we can see that the films are actually slightly thinner as we move toward the edge of the substrate holder.

The addition of the hydrogen during the sputtering procedure has been reported to cause a drop in the ionization discharge and Ar^+ ion densities [35–37]. Some have also reported yield reduction with the introduction of hydrogen [38–40] due to the low mass of hydrogen, and this may explain why we had a slightly thinner coating on the edge region if hydrogen bombardment of the target and its consecutive incorporation into the lattice behaved selectively, depending on the position of the sample.

Hence, we can continue with our original assumption where we stated that more hydrogen atoms are doped into ZnO lattice at the edge of the substrate holder and oxygen vacancy alone is not a determining factor.

For a TCO material to be suitable for most electrode applications, as well as the electrical resistivity (ϱ), the optical absorption should be minimised [41]. The overall sheet resistance of the ZnO samples based on their position on the substrate holder is presented in Figure 5.

We evaluated all the ZnO samples with UV–Vis spectroscopy, and the absorption properties of the films are presented in Figure 7.

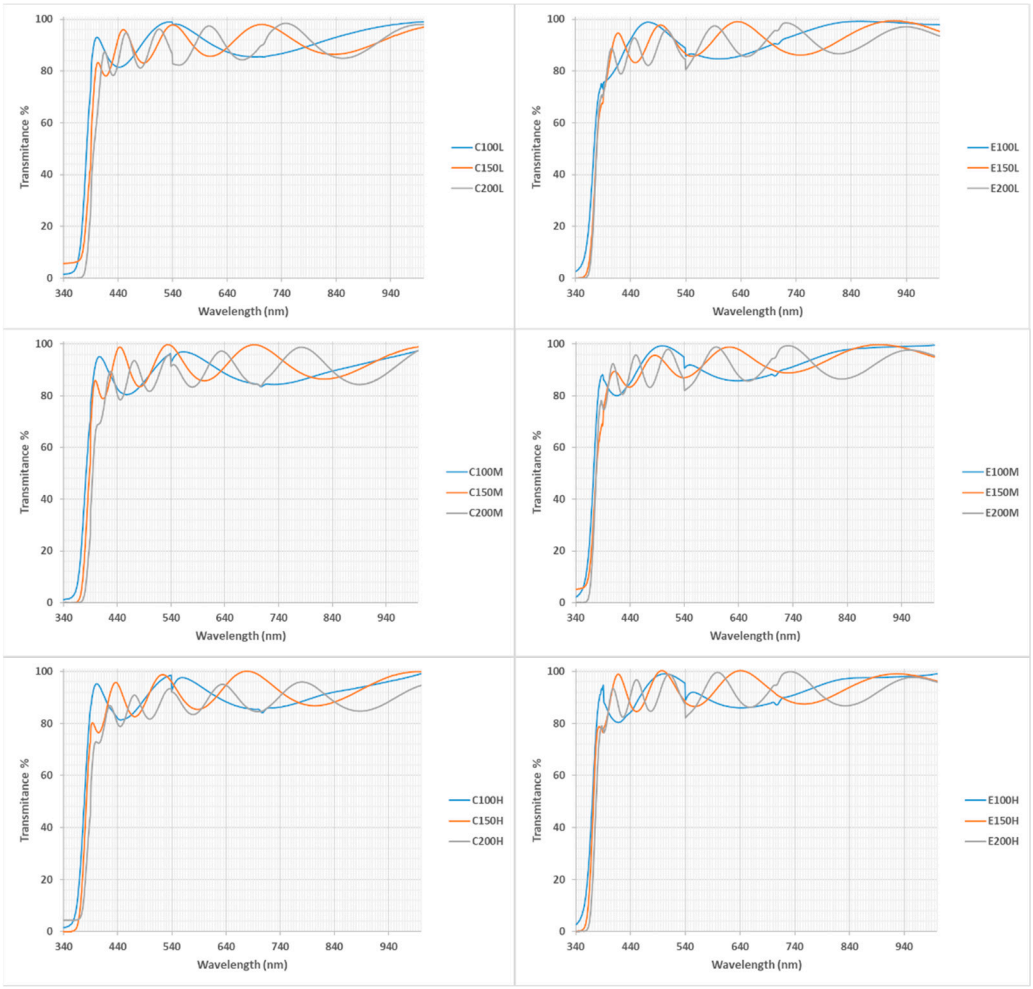

Figure 7. The transmittance spectra of the ZnO thin films obtained via UV–Vis spectroscopy. All samples demonstrate above 80% transmittance between 400 nm and 1000 nm.

The data presented in Figures 5 and 7 clearly demonstrated the potential of ZnO as an alternative TCO without the need for indium or any other metal doping, if the position of the substrate with respect to the plasma is considered. The optical band gap of the deposited thin films was obtained via the Tauc plot method, the results are presented in Table 2 for edge- and centre-deposited ZnO thin films.

Table 2. The optical band gap of the ZnO samples deposited at various conditions, comparing the results obtained from samples positioned on the edge and centre of the substrate holder. The samples prepared on the edge also demonstrate a slightly higher band gap.

Centre	Optical band gap (eV)	Edge	Optical band gap (eV)
C100H	3.3	E100H	3.4
C150H	3.300	E150H	3.4
C200H	3.200	E200H	3.38
C100M	3.300	E100M	3.37
C150M	3.290	E150M	3.3
C200M	3.320	E200M	3.39
C100L	3.250	E100L	3.35
C150L	3.200	E150L	3.39
C200L	3.220	E200L	3.35
Average	3.264		3.37
SD	0.047		0.032

3.3. Analysis of the Plasma Emissions

We examined the plasma emissions at the surface of the target as described in the experimental section. We carried out a comparative study with an IZO target fitted on the magnetron to evaluate the variation in plasma emissions comparing the two targets (IZO and ZnO), considering that with the IZO sample we were not observing a drastic variation of electrical properties associated with sample position (Figure 4).

The emissions from the plasma generate numerous emission peaks, and the ratio of these peaks is classically associated with plasma conditions. However, although peak intensities varied from centre to edge, observations purely based on the spectral plot did not indicate an easily identifiable variation between the two materials. To illustrate this, the data representing the emission of the plasma at 100 watts under a 10 sccm flow rate for the ZnO and IZO targets are presented in Figure 8.

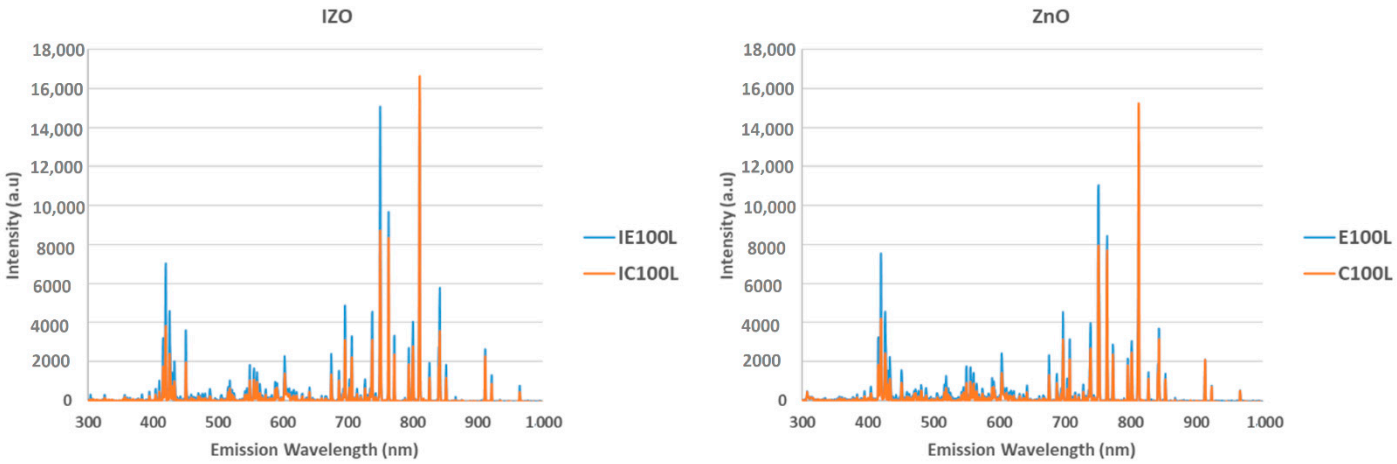

Figure 8. The spectral emission of the plasma at 100 watts of power under a 6 sccm flow rate at the edge (blue) and centre (orange) of the target for the IZO (**left**) and ZnO (**right**) targets.

In Figure 8 we can see that the intensity of various peaks is higher at the edge of the target surface compared to the centre region. These emissions are associated with various atomic transition in the plasma. The increase in intensity at the edge is due to the way that the magnetron operates, given the magnets installed in it, leading to an area with higher ion bombardment rate [42]. It is possible to analyse every peak intensity and to obtain certain parameters such as the electron temperature from the data, which is a time intensive approach and beyond the scope of this report. Instead, we implemented our simpler

assessment based on the colour function parameters of the plasma at the centre and edge region of the target based on our previous report. This simple approach was applied to evaluate an overall change in the plasma condition. The colour functions of the plasma light at the centre and edge regions were calculated and are presented in Figure 9. Using this approach, the difference in plasma conditions became more apparent to the naked eye. The colour functions could represent the overall macro environment of the plasma constituents without indulging in deep physics and statistical mechanics associated with evaluating a plasma.

In our approach, we can now consider each colour coordinate associated with a particular plasma emission condition on each target as a vector defined by the "x" and "y" colour coordinates.

Once we defined the coordinates as vectors associated with data obtained for the edge or centre, we calculated the angular rotation of each vector associated with the shift observed from the edge to the centre.

We calculated this angular rotation, and these results are presented in Figure 10.

The data presented in Figure 10 showed that the angular rotation associated with vectors representing the "x" and "y" colour functions associated with the edge compared to the centre showed up to eight times more variation (from edge to centre) in the ZnO target compared to the IZO target. This method of plasma analysis is not mature yet and cannot lead to an absolute conclusion; however, it gives us some indication that the IZO target showed a more homogenous plasma condition across the target surface compared to the ZnO target.

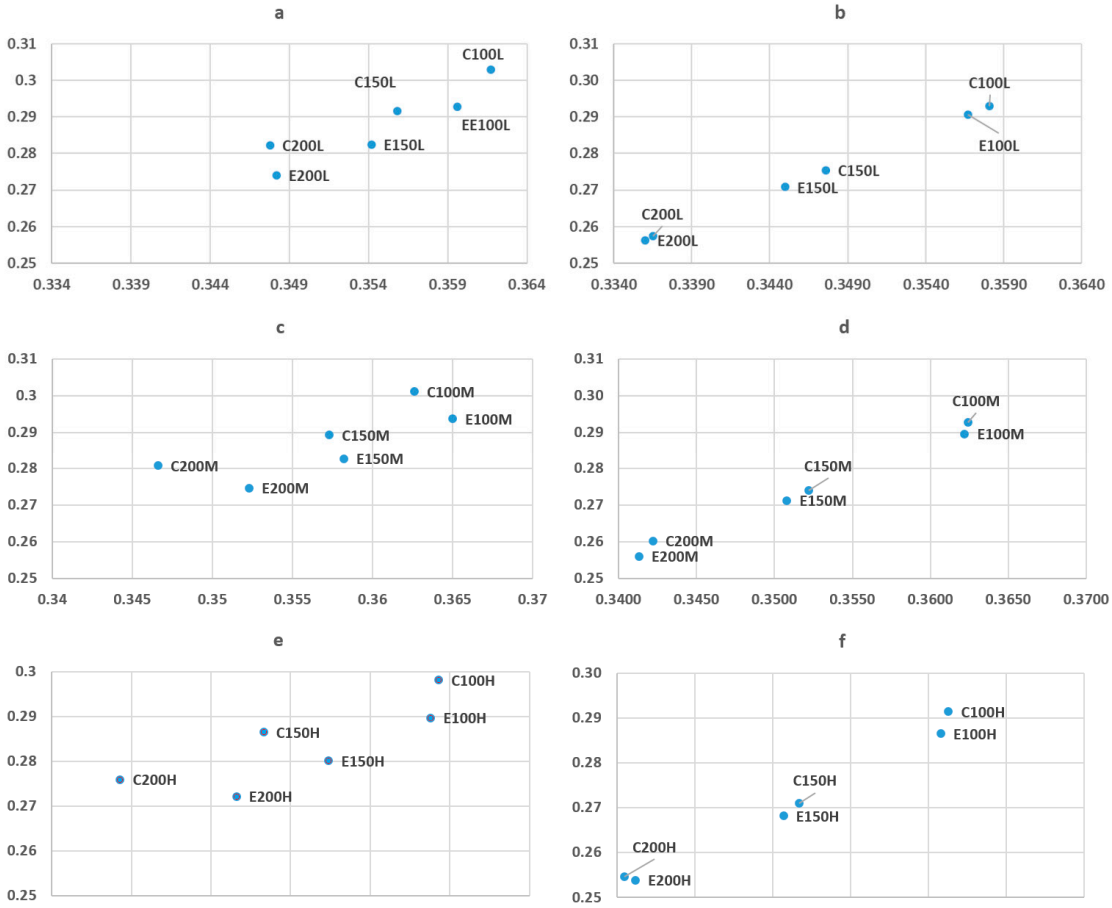

Figure 9. The x and y chromaticity index of the plasma light at the edge (E) and the centre (C) of the target for ZnO and IZO at various gas flow rates and plasma powers (100, 150 and 200 Watts) is plotted. With this approach, the difference in the plasma condition becomes more apparent to the naked eye. a: ZnO; b: IZO samples with 6 sccm flow rate; c: ZnO; d: IZO samples with 10 sccm flow rates and e: ZnO; f: IZO samples with 13.9 sccm flow rates of argon/hydrogen gas.

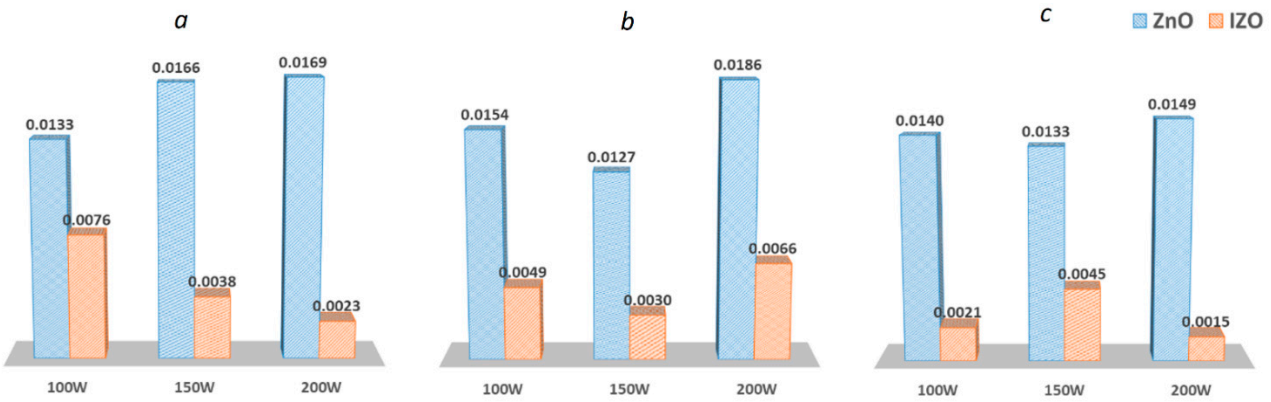

Figure 10. The angular rotation (the angle between the associated edge and centre vectors) of the "x" and "y" coordinate vectors representing the colour functions associated with the plasma conditions during the deposition of IZO and ZnO samples deposited under gas flow rates of a: 13.9 sccm; b: 10 sccm and c: 6sccm.

To further examine the emission spectrum properties leading to the variation in "x" and "y" colour coordinates of ZnO and IZO samples, the total area under the emission peaks (integral) of the plasma was calculated by Plasus Emicon software. We then assessed the ratio of area under emission at 100 nm intervals from 300 to 900 nm of the emission to the total emission area. This analysis was carried out for all the experimental procedures discussed so far associated with ZnO and IZO targets.

The ratio of area under emission peaks at 100 nm interval over the total area under the whole emission spectrum are presented in Figure 11, where the emission ratios for each section associated with the centre and edge of the target surface (ZnO and IZO) are plotted. The main differences between the ZnO and IZO target were in the A, C and D section of the spectrum corresponding to the 500–600 and 600–700 nm emission wavelengths.

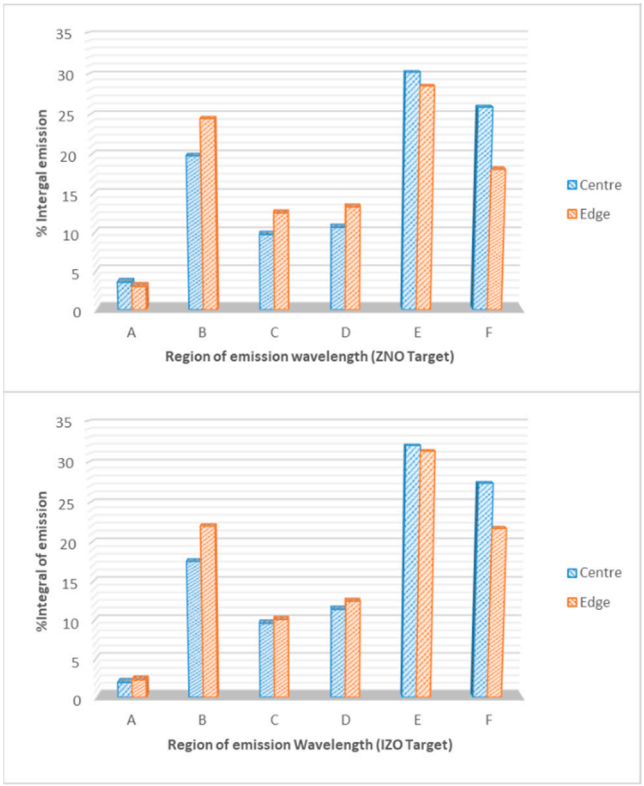

Figure 11. Comparing the area under emission peaks associated with 100 nm interval segments of the plasma spectrum to the whole spectrum for ZnO and IZO samples at the edge and centre.

From the results presented so far, although we see certain variation between the emission patterns associated with ZnO and IZO targets, the variations are interesting but do not seem to be conclusive for explaining the observed variation in electrical conductivity of ZnO and IZO as presented in Figure 4. An in-depth peak ratio analysis can be performed to gain insights into the physical parameters of the plasma, such as electron temperature; however, in the current report we focus on describing the observations and such studies require a separate dedicated study report.

Up to this point, we can assume that the hydrogen impurity incorporation within a ZnO or IZO lattice follows a certain reduced gradient from the edge to the centre. The hydrogen impurity can be either interstitial or substitutional. The H+ in the ZnO system will occupy locations within the lattice, where it can bind to an oxygen atom and form an O–H bond. Considering substitutional hydrogen, it is located in the proximity of a nominal oxygen position within the lattice and behaves as a shallow donor [18]. The donor behaviour of the hydrogen impurity in ZnO clearly explains the conductivity observed in ZnO systems and improvement of IZO conductivity.

This implies that we need to consider the state of the materials during their transport from the target surface to the substrate. From these results, and reported studies discussed, we can assume that the ZnO particles that form on the substrate surface have more hydrogen content at the edge location compared to the centre region of the substrate holder. This observation can possibly be explained considering the following concepts and assumptions:

- Firstly, hydrogen ions (along with argon ions) bombard the surface of the target material, resulting in ejection of surface atoms from the surface of the target, while some of these ions will also integrate into the target material.
- Secondly, the integration of the hydrogen into the surface of the target material as discussed and based on referenced literature may lead to formation of regions at the target surface possessing complex magnetic behaviour.

One way of explaining the observations reported in this study is to consider previously reported studies where angular dependency of thin films depositions via the sputtering process were investigated. During the sputtering deposition process it has been shown that geometrical shadowing of an incident beam by the existing protruding parts of the growing surface profoundly affect the deposition's morphology [43]. This is referred to as competitive shadowing, which can affect the properties of the thin films, in particular step coverage and microelectronic properties [44]. In a more recent study, Hippler et al. [45] carried out a study on the angular dependence of plasma parameters and thin film properties focusing on titanium and titanium oxide layers deposited via HIPIMS. They performed separate reactive (argon/oxygen) and non-reactive depositions regimes using a Langmuir probe and substrates at various angular positions (0°,30°,60° and 80°) with respect to the target [45]. In their study, significant variations in electron density were reported depending on the reactive or non-reactive experimental regime, with the non-reactive regime showing up to five times larger electron density values. They also measured the mean electron energy (pulse time dependent), which demonstrated similar values between the two regimes. However, most interesting are the values they demonstrated depending on the substrate position with respect to the target, which finds significant relevance with our observations. Both electron density and mean electron energy values are reduced at wider incident angles on the target surface. It should be noted that our study needs to be repeated mimicking the experimental protocols carried out by Hippler et al., something that we are very interested to pursue. Considering the observations reported here, such studies will give a significant perspective in understanding the formation of the conductive zinc oxide films in presence of hydrogen during the sputtering process. However, at this stage, based on the above reported research, if incorporation of the hydrogen into the target material leads to formation of surfaces at the target with complex magnetic behaviours, then it may result in the target material itself interfering with

the magnetron's magnetic fields and as such creating electron density and electron energy values dependent on angular incidence on the target surface. The time dependency studies on plasma potential reported by Hippler et al. at various angular positions can also be influenced by the target surface gaining magnetic properties as well as due to the overall interaction of electron and ions in such a complex magnetic environment.

Parallel to the above discussion, it has been reported that the sputtered flux from an ion bombarded target surface is composed of atoms, polyatomic molecules and clusters [46–48], and various models have been proposed to describe the sputtering of small clusters and molecules [49–55]. If we assume that during the sputtering process, molecular ejection from the target surface occurs, there will be a flux of both pure ZnO and hydrogen doped ZnO leaving the target surface with various speeds and randomly dispersed direction vectors. As discussed, hydrogenated ZnO nanoparticles have been shown to demonstrate ferromagnetism.

Hypothetically, the hydrogen doped ZnO particles possessing ferromagnetic properties are affected by the magnetic field of the magnetron's magnets. This effect creates additional vector forces that ultimately promote the ferromagnetic hydrogen doped ZnO to the edge of the target, while the non-ferromagnetic pure ZnO particles are condensed randomly across the substrate holder. This model is illustrated in Figure 12, where we take the very simple approach of considering a certain number of small particles with a magnetic moment along a magnetic field between the N and S poles of the magnetron's magnet. Upon surface bombardment of the target with Ar/H ions, the target atoms acquire kinetic energy for travel to the surface of the substrate. If these particles possess ferromagnetic properties as we have hypothesised, then there is dipole–dipole interaction that needs to be considered in this model; an attractive and repulsive force vector will exist as these magnetic particles interact with the field and their geometrical orientation within space. This vector either will combine with the initial vector or will counter it depending on the particles' positions, according to Equations (1)–(4).

$$U = -MB\ \cos\theta \tag{1}$$

$$\mathrm{B} = \frac{\mu}{4\pi} \times \frac{nM}{R^3} \tag{2}$$

$$T = -MB \sin\theta \tag{3}$$

$$\mathrm{Force} = -\frac{dU}{dR} \tag{4}$$

Considering the interaction of two hypothetical magnets alfa and beta, in these equations, U is the potential energy of a magnet "*alpha*" exposed to the magnetic field of magnet "*beta*". B is the magnetic field of the magnet *alpha*, M is the magnetic momentum, θ is the angle between the axial angle of the magnetic moment of a magnetic dipole and the magnetic field generated by the magnetron magnet, R is the distance between the centres of the two magnets and F is force imposed on *alpha*. Considering these equations, we can see that the angular geometry of one magnet to another as well as its location in space can lead to positive to negative values of force. Considering this and assuming the hypothetical magnetic particles depicted in Figure 12, the difference between the point c1/b1 and c2/b2 is the magnetic field gradient. In the central position, the magnetic field gradient is higher than in the edge positions. Then, the attractive magnetic force will be higher in the centre than in the edges. Particles at points b2 and c2 will experience a more complex magnetic environment countering their velocity away from the target surface. The gas

flow rate, which technically translates to the working chamber pressure and the plasma power, which translates to the kinetic energy of the sputtered particles, will affect the process such that at higher chamber pressures, the probability of particle collisions increases, while higher plasma power leads to higher energy particles, which will be less influenced by the magnetic complexity described. The effect of higher kinetic energy overcoming the magnetic complexity can be seen in Figure 5, where higher plasma power results in deposition of more conductive films at the edge region of the substrate holder. Higher chamber pressure would also result in more particles interacting with the magnetrons magnetic field, and as such may reduce the effect of the field with respect to sputtered particles; however, such conclusions require extensive analysis of the magnetic fields during the experiment, which is beyond the scope of this report.

We can propose the following hypothesis to explain the experimental observations: during the sputtering process, due to complex magnetic dipole interactions, hydrogen doped ZnO particles leaving the target surface tend to accumulate on the edges of the substrate holder region. This results in thin films with better electrical conductivity, while at the centre, ZnO particles that do not possess magnetic properties are more predominant, and as such, samples prepared in the centre location of the substrate holder are less conductive.

This process occurs both in IZO and ZnO targets, hence the samples prepared at the edge of the substrate demonstrate higher conductivity due to the higher hydrogen doping. In IZO samples, however, since the presence of indium already acts as a carrier concentration enhancer, we see a slight improvement in conductivity; however, in ZnO samples, because only hydrogen acts as the electron donor in the lattice, we see the large variation of conductivity gradient from the edge to the centre.

However, this work needs to be followed up with simulation studies and more in depth experimental work to verify the hypothesis proposed here, and the authors are planning explore this study further accordingly. The magnetron in this study had a balanced magnetic set up; our plan for future studies will be to carry out the experiments with unbalanced magnetic and no magnet set up magnetron systems.

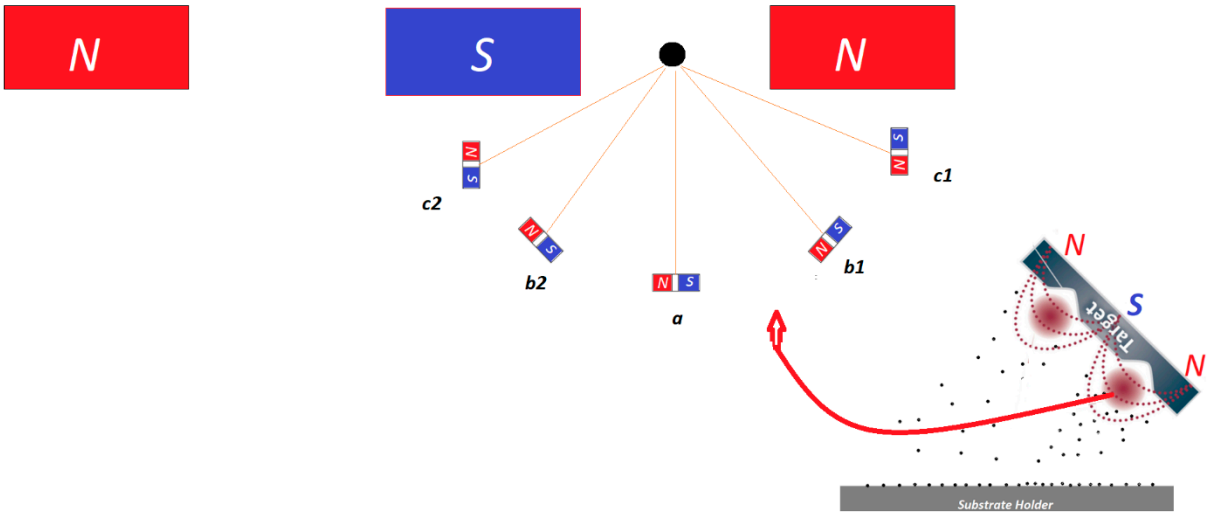

Figure 12. A simple approach of considering a certain number of small particles with a magnetic moment along a magnetic field between the N and S poles of the magnetron's magnet. The angle between the centres of the magnets and their position defines how the larger magnet affects them.

4. Conclusions

This study primarily is a report of observations associated with deposition of zinc oxide films in the presence of hydrogen along with argon and will require further studies to validate the assumptions and hypothetical statements in this report, particularly similar

experiments to that described by Hippler et al. We demonstrated that it is possible to produce highly conductive ZnO thin films doped with hydrogen at room temperature. The films possess acceptable optical band gap and as such demonstrate above 80% transmittance and best sheet resistance of ~18 Ω square (E200 samples). However, the procedure requires certain precisions in terms of substrate positioning and its trajectory with the magnetron.

We also demonstrated the potential of assessing the sputtering plasma via colour function analysis, based on evaluating the specific ratios of area under emission peaks as a tool for monitoring the status of plasma during sputtering procedures. This method does not require precise plasma analysis and complex calculations when detailed study of the plasma is not required and instead provides the operator with an easy to understand observing parameter as an indicator of sputtering plasma status.

The hypothesis proposed on the ferromagnetic properties of the sputtered ZnO particles requires further examination and will require detailed analysis of the hydrogen doping variations with balanced and unbalanced magnetron configurations to validate our conjecture. The integration of hydrogen into the target is an area that should be explored further to assess this hypothesis in future attempts. It is an interesting topic to explore by us and other researchers interested in the field.

Author Contributions: Conceptualization, A.S.; methodology, A.S.; software, A.H.; validation, H.U., A.S. and A.H.; formal analysis, A.S; investigation, A.S.; resources, H.U.; data curation, A.A.; writing—original draft preparation, A.S.; writing—review and editing, A.A. and A.H; visualization, A.S.; supervision, H.U.; project administration, A.S.; funding acquisition, H.U. All authors have read and agreed to the published version of the manuscript.

Funding: This research was funded by Grand Challenge Research Fund (GCRF)/EPSRC toward the SUNRISE program, No. EP/P032591/1.

Data Availability Statement: No new data were created or analyzed in this study. Data sharing is not applicable to this article.

Conflicts of Interest: The authors declare no conflict of interest.

References

1. Ginley, D.S.; Hosono, H.; Paine, D.C. *Handbook of Transparent Conductors*; Springer: Berlin, Germany, 2011; pp. 353–425.
2. Ginley, D.S.; Bright, C. Transparent Conducting Oxides. *MRS Bull.* **2000**, *25*, 15–18, doi:10.1557/mrs2000.256.
3. Hosono, H. Recent progress in transparent oxide semiconductors: Materials and device application. *Thin Solid Films* **2007**, *515*, 6000–6014, doi:10.1016/j.tsf.2006.12.125.
4. Ellmer, K. Past achievements and future challenges in the development of optically transparent electrodes. *Nat. Photon* **2012**, *6*, 809–817, doi:10.1038/nphoton.2012.282.
5. Granqvist, C.G. Transparent conductors as solar energy materials: A panoramic review. *Sol. Energy Mater. Sol. Cells* **2007**, *91*, 1529–1598, doi:10.1016/j.solmat.2007.04.031.
6. King, P.; Veal, T.D. Conductivity in transparent oxide semiconductors. *J. Physics: Condens. Matter* **2011**, *23*, 334214, doi:10.1088/0953-8984/23/33/334214.
7. Calnan, S.; Tiwari, A.N. High mobility transparent conducting oxides for thin film solar cells. *Thin Solid Films* **2010**, *518*, 1839–1849, doi:10.1016/j.tsf.2009.09.044.
8. Khachatryan, H.; Kim, D.J.; Kim, M.; Kim, H.-K. Roll-to-Roll fabrication of ITO thin film for flexible optoelectronics appli-cations: The role of post-annealing. *Mater. Sci. Semicond. Process* **2018**, *88*, 51–56.
9. Morales-Masis, M.; De Nicolas, S.M.; Holovsky, J.; De Wolf, S.; Ballif, C. Low-Temperature High-Mobility Amorphous IZO for Silicon Heterojunction Solar Cells. *IEEE J. Photovoltaics* **2015**, *5*, 1340–1347, doi:10.1109/jphotov.2015.2450993.
10. Martins, R.; Almeida, P.; Barquinha, P.; Pereira, L.; Pimentel, A.; Ferreira, I.; Fortunato, E. Electron transport and optical characterization amorphous indium zinc oxide films. *J. Non Cryst. Solids* **2006**, *352*, 1471–1474.
11. Taylor, M.P.; Readey, D.W.; Van Hest, M.F.A.M.; Teplin, C.W.; Alleman, J.L.; Dabney, M.S.; Gedvilas, L.M.; Keyes, B.M.; To, B.; Perkins, J.D.; et al. The remarkable thermal stability of amorphous In-Zn-O transparent conductors. *Adv. Funct. Mater.* **2008**, *18*, 3169–3178, doi:10.1002/adfm.200700604.
12. Park, Y.R.; Nam, E.-K.; Boo, J.-H.; Jung, D.-G.; Suh, S.-J.; Kim, Y.-S. Hydrogenated In-doped ZnO thin films for the new anode material of organic light-emitting devices: Synthesis and application test. *Bull. Korean Chem. Soc.* **2007**, *28*, 2396–2400.
13. Park, Y.R.; Kim, J.; Kim, Y.S. Growth and characteristics of hydrogenated In-doped ZnO thin films by pulsed DC magnetron sputtering. *Appl. Surf. Sci.* **2009**, *256*, 1589–1594, doi:10.1016/j.apsusc.2009.09.026.

14. Bädeker, K. The electrical conductivity and thermoelectric power of some heavy metal compounds. *Annal. Physik*. **1907**, *327*, 749–766.
15. Minami, T. New n-type transparent conducting oxides. *MRS Bull.* **2000**, *25*, 38–44, doi:10.1557/mrs2000.149.
16. Mollwo, E. The effect of hydrogen on the conductivity and luminescence of zinc oxide crystals. *Z. Physik*. **1954**, *138*, 478–488.
17. Thomas, D.G.; Lander, J.J. Hydrogen as a Donor in Zinc Oxide. *J. Chem. Phys.* **1956**, *25*, 1136–1142, doi:10.1063/1.1743165.
18. Van de Walle, C.G. Hydrogen as a Cause of Doping in Zinc Oxide. *Phys. Rev. Lett*. **2000**, *85*, 1012–1015.
19. Kohan, F.; Ceder, G.; Morgan, D.; Van de Walle, C.G. First-principles study of native point defects in ZnO. *Phys. Rev. B* **2000**, *61*, 15019.
20. Hofmann, D.M.; Hofstaetter, A.; Leiter, F.; Zhou, H.; Henecker, F.; Meyer, B.K.; Orlinskii, S.B.; Schmidt, J.; Baranov, P.G. Hydrogen: A Relevant Shallow Donor in Zinc Oxide. *Phys. Rev. Lett.* **2002**, *88*, 045504, doi:10.1103/physrevlett.88.045504.
21. Cox, S.F.J.; Davis, E.A.; Cottrell, S.P.; King, P.J.C.; Lord, J.S.; Gil, J.M.; Alberto, H.V.; Vilão, R.C.; Duarte, J.P.; De Campos, N.A.; et al. Experimental Confirmation of the Predicted Shallow Donor Hydrogen State in Zinc Oxide. *Phys. Rev. Lett.* **2001**, *86*, 2601–2604, doi:10.1103/physrevlett.86.2601.
22. Van de Walle, C.G. Hydrogen as a shallow centre in semiconductors and oxides. *Phys. Status Solidi b* **2003**, *235*, 89–95.
23. Hosono, H.; Ueda, K. Transparent Conductive Oxides. In *Springer Handbook of Electronic and Photonic Materials*; Springer: Berlin, Germany, 2017; doi:10.1007/978-3-319-48933-9_58.
24. Yan, X.; Tian, L.; Tan, X.; Zhou, M.; Liu, L.; Chen, X. Modifying oxide nanomaterials' properties by hydrogenation. *MRS Commun.* **2016**, *6*, 192–203, doi:10.1557/mrc.2016.33.
25. Li, T.; Ong, C.S.; Herng, T.S.; Yi, J.; Bao, N.; Xue, J.M.; Feng, Y.P.; Ding, J. Surface ferromagnetism in hydrogenated-ZnO film. *Appl. Phys. Lett.* **2011**, *98*.
26. Park, J.K.; Kwon, H.-J.; Lee, C.E. NMR Observation of Mobile Protons in Proton-Implanted ZnO Nanorods. *Sci. Rep.* **2016**, *6*, 23378, doi:10.1038/srep23378.
27. Robaina, O.V.; Cabrera, A.F.; Meyer, M.; Romano, R.M.; Cruz, A.F.; Torres, C.E.R. Room-Temperature Ferromagnetism Induced by High-Pressure Hydrogenation of ZnO. *J. Phys. Chem. C* **2019**, *123*, 19851–19861, doi:10.1021/acs.jpcc.9b04902.
28. Esquinazi, P.; Hergert, W.; Spemann, D.; Setzer, A.; Ernst, A. Defect-Induced Magnetism in Solids. *IEEE Trans. Magn.* **2013**, *49*, 4668–4674, doi:10.1109/tmag.2013.2255867.
29. Salimian, A.; Hasnath, A.; Anguilano, L.; Onwukwe, U.; Aminishahsavarani, A.; Sachez, C.; Upadhyaya, H. Highly Conductive Zinc Oxide Based Transparent Conductive Oxide Films Prepared Using RF Plasma Sputtering Under Reducing Atmosphere. *Coatings* **2020**, *10*, 472, doi:10.3390/coatings10050472.
30. Salimian, A.; Haghpanahan, R.; Hasnath, A.; Upadhyaya, H. Optical analysis of RF sputtering plasma through colour characterization. *Coatings* **2019**, *9*, 315.
31. Hautier, G.; Miglio, A.; Waroquiers, D.; Rignanese, G.-M.; Gonze, X. How Does Chemistry Influence Electron Effective Mass in Oxides? A High-Throughput Computational Analysis. *Chem. Mater.* **2014**, *26*, 5447–5458, doi:10.1021/cm404079a.
32. Wallinga, J.; Arnoldbik, W.M.; Vredenberg, A.M.; Schropp, R.E.I.; Van Der Weg, W.F. Reduction of Tin Oxide by Hydrogen Radicals. *J. Phys. Chem. B* **1998**, *102*, 6219–6224, doi:10.1021/jp981447l.
33. De Wit, J. Electrical properties of In2O3. *J. Solid State Chem.* **1973**, *8*, 142–149, doi:10.1016/0022-4596(73)90007-8.
34. Dewit, J.H.W., Vanunen, G., Lahey, M., Electron concentration and mobility in In2O3. *J. Phys. Chem. Solids* **1997**, *38*, 819-824.
35. Gordon, M.H., Kruger, C.H. Non-equilibrium effects of diluent addition in recombining argon plasma. *Phys. Fluids B Plasma Phys.* **1993**, *5*, 1014.
36. Meulenbroeks, R.F.G.; Van Beek, A.J.; Van Helvoort, A.J.G.; Van De Sanden, M.C.M.; Schram, D.C. Argon-hydrogen plasma jet investigated by active and passive spectroscopic means. *Phys. Rev. E* **1994**, *49*, 4397–4406, doi:10.1103/physreve.49.4397.
37. Mason, R.S.; Miller, P.D.; Mortimer, I.P. Anomalous loss of ionization in argon-hydrogen plasma studied by fast flow glow discharge mass spectrometry. *Phys. Rev. E* **1997**, *55*, 7462–7472, doi:10.1103/PhysRevE.55.7462.
38. Tabares, F.L., Tafalla, D. Sputtering of metallic walls in Ar/H2 direct current glow discharges at room temperature. *J. Vac. Sci. Technol. A* **1996**, *14*, 3087–3091.
39. Budtz-Jorgensen, C.V., Kringhoj, P., Bottiger, J. The critical role of hydrogen for physical sputtering with Ar–H2 glow discharges. *Surf. Coat. Technol*. **1999**, *116*, 938–943.
40. Smithwick, R.W., III; Lynch, D.W.; Franklin, J.C. Relative ion yields measured with a high-resolution glow discharge mass spectrometer operated with an argon/hydrogen mixture *J. Am. Soc. Mass Spectrom*. **1993**, *4*, 278–285.
41. Knewstubb, P.F.; Tickner, A.W. Mass Spectrometry of Ions in Glow Discharges. I. Apparatus and Its Application to the Positive Column in Rare Gases. *J. Chem. Phys.* **1962**, *36*, 674–683, doi:10.1063/1.1732592.
42. Luo, S.; Kohiki, S.; Okada, K.; Kohno, A.; Tajiri, T.; Arai, M.; Ishii, S.; Sekiba, D.; Mitome, M.; Shoji, F. Effects of Hydrogen in Working Gas on Valence States of Oxygen in Sputter-Deposited Indium Tin Oxide Thin Films. *ACS Appl. Mater. Interfaces* **2010**, *2*, 663–668, doi:10.1021/am9006676.
43. Bales, G.S.; Bruinsma, R.; Eklund, E.A.; Karunasiri, R.P.U.; Rudnick, J.; Zangwill, A. Growth and Erosion of Thin Solid Films. *Science* **1990**, *249*, 264–268, doi:10.1126/science.249.4966.264.
44. Horkel, M.; van Aeken, K.; Eisenmenger-Sittner, C.; Depla, D.; Mahieu, S.; Leroy, W.P. Experimental determination and simulation of the angular disruption of the metal flux during magnetron sputter deposition. *J. Phys. D Appl. Phys*. **2010**, *43*.

45. Hippler, R.; Hubicka, Z.; Cada, M.; Ksirova, P.; Wulff, H.; Helm, C.A.; Stranak, V. Angular dependence of plasma parameters and film properties during high power impulse magnetron sputtering for deposition of Ti and TiO_2 layers. *J. Appl. Phys.* **2017**, *121*, 171906, doi:10.1063/1.4977823.
46. Hofer, W.O. Angular, energy, and mass distribution of sputtered particles. In *Sputtering by Particle Bombardment III*; Behrisch, R., Wirrmaack, K., Eds; Springer: Berlin/Heidelberg, Germany, 1991; Volume 64, p. 15
47. Urbassek, H.M.; Hofer, W.O. Sputtering of molecules and clusters. *Mat. Fys. Medd*. **1993**, *43*, 97–125.
48. Sundqvist, B.U.R. Desorption of organic molecules from solid and liquid surfaces induced by particle impact. In *Sputtering by Particle Bombardment III*; Behrisch, R., Wirrmaack, K., Eds; Springer: Berlin/Heidelberg, Germany, 1991; Volume 64, p. 257.
49. Gerhard, W.; Villalba, V.; Maggiolo, A.R. A model calculation of the neutral molecule emission by sputtering processes. *Eur. Phys. J. B* **1975**, *22*, 31–39, doi:10.1007/bf01325457.
50. Können, G.P.; Tip, A.; De Vries, A.E. On the energy distribution of sputtered dimers. *Radiant Eff.* **1974**, *21*, 269–274, doi:10.1080/00337577408232416.
51. Konnen, G.P.; Tip, A.; de Vries, A.E. On the energy distribution of sputtered Clustrs. *Radiant. Eff*. **1975**, *26*, 23–29.
52. Honda, F.; Lancaster, G.M.; Fukuda, Y.; Rabalais, J.W. SIMS study of the mechanism of cluster formation during ion bombardment of alkali halides. *J. Chem. Phys.* **1978**, *69*, 4931–4937, doi:10.1063/1.436480.
53. Galera, R.; Blais, J.; Bolbach, G. Molecular sputtering and damage induced by kiloelectron ions in organic monolayer—Metal systems. *Int. J. Mass Spectrom. Ion Process.* **1991**, *107*, 531–543, doi:10.1016/0168-1176(91)80046-p.
54. Haff, P.K.; Watson, C.C.; Yung, Y.L. Sputter ejection of matter from Io. *J. Geophys. Res. Space Phys.* **1981**, *86*, 6933–6938, doi:10.1029/ja086ia08p06933.
55. King, B.V.; Ziv, A.R.;Lin, S.H.; Tsong, I.S.T.; Mass distribution of ejected molecules and clusters in nanocascade sputtering processes. *J. Chem. Phys*. **1985**, *82*, 3641–3645.